ARL-TN-1128 ● AUG 2022

High-Speed Army Reference Vehicle

by Joseph D Vasile, Frank Fresconi, James DeSpirito, Marco Duca, Thomas Recchia, Brian Grantham, Rodney D W Bowersox, and Edward B White

NOTICES

Disclaimers

ARL-TN-1128 ● AUG 2022

High-Speed Army Reference Vehicle

Joseph D Vasile, Frank Fresconi, and James DeSpirito
DEVCOM Army Research Laboratory

Marco Duca and Thomas Recchia
DEVCOM Armaments Center

Brian Grantham
DEVCOM Aviation & Missile Center

Rodney D W Bowersox and Edward B White
Texas A&M University

REPORT DOCUMENTATION PAGE	*Form Approved* *OMB No. 0704-0188*

1. REPORT DATE *(DD-MM-YYYY)*	August 2022
2. REPORT TYPE	Technical Note
3. DATES COVERED (From - To)	1 April–1 November 2020
4. TITLE AND SUBTITLE	High-Speed Army Reference Vehicle
5a. CONTRACT NUMBER	
5b. GRANT NUMBER	
5c. PROGRAM ELEMENT NUMBER	
6. AUTHOR(S)	Joseph D Vasile, Frank Fresconi, James DeSpirito, Marco Duca, Thomas Recchia, Brian Grantham, Rodney D W Bowersox, and Edward B White
5d. PROJECT NUMBER	
5e. TASK NUMBER	
5f. WORK UNIT NUMBER	
7. PERFORMING ORGANIZATION NAME(S) AND ADDRESS(ES)	DEVCOM Army Research Laboratory ATTN: FCDD-RLW-WD Aberdeen Proving Ground, MD 21005
8. PERFORMING ORGANIZATION REPORT NUMBER	ARL-TN-1128
9. SPONSORING/MONITORING AGENCY NAME(S) AND ADDRESS(ES)	
10. SPONSOR/MONITOR'S ACRONYM(S)	
11. SPONSOR/MONITOR'S REPORT NUMBER(S)	
12. DISTRIBUTION/AVAILABILITY STATEMENT	Approved for public release: distribution unlimited.
13. SUPPLEMENTARY NOTES	ORCID ID: Joseph Vasile, 0000-0003-3812-6277

14. ABSTRACT

The US Army recently formulated a strategy regarding how the future Army will fight and the associated modernization and research priorities for achieving these military capabilities. Long-Range Precision Fires underpinned by hypersonic flight are critical to ensuring that the United States can enforce its will against any competitor. Many barriers must be overcome to realize an effective future US Army. Some of these gaps are in understanding hypersonic vehicle aerothermodynamics, thus motivating the need for foundational research. The goal of this report is to define a canonical, Army-relevant configuration suitable for foundational research to allow for focused collaboration with a critical mass of appropriate subject matter experts. Data and knowledge gained from studies on this open geometrical configuration may be subject to more restrictive distribution.

15. SUBJECT TERMS

long-range projectiles, high-speed flight vehicle, Army reference vehicle, hypersonic flight, Long-Range Precision Fires

16. SECURITY CLASSIFICATION OF:			17. LIMITATION OF ABSTRACT	18. NUMBER OF PAGES	19a. NAME OF RESPONSIBLE PERSON
					Joseph Vasile
a. REPORT	b. ABSTRACT	c. THIS PAGE			19b. TELEPHONE NUMBER (Include area code)
Unclassified	Unclassified	Unclassified	UU	21	(410) 306-1794

Standard Form 298 (Rev. 8/98)
Prescribed by ANSI Std. Z39.18

Contents

List of Figures

Acknowledgments

The High-Speed Army Reference Vehicle (HARV) was shaped and designed via a cooperative agreement between DEVCOM ARL and the Texas A&M University System Bush Combat Development Complex in support of Army Futures Command and the University Technology Development Division (Contract No. W911NF1920243). The authors would like to thank Mr Ilmars Celmins, from DEVCOM ARL, for producing mechanical drawings and schematics of HARV.

1. Introduction

The US Army recently formulated a strategy regarding how the future Army will fight and the associated modernization and research priorities for achieving these military capabilities.[1,2] Long-Range Precision Fires underpinned by hypersonic flight are critical to ensuring that the United States can enforce its will against any competitor.

Many barriers must be overcome to realize an effective future US Army. Some of these gaps are in understanding hypersonic vehicle aerothermodynamics, thus motivating the need for foundational research. Lack of predictive knowledge of the complex physics and chemistry occurring around hypersonic vehicles inhibits timely, optimized multi-component design. Specific phenomena that are poorly understood include boundary layer transition and shock–boundary layer interactions. The inability to properly model phenomenon yields uncertainty in characteristics, such as the surface pressure distribution and heat flux, which negatively impact vehicle technologies including stability, control, and thermal load management.

Fortunately, a precedent exists for promoting community-wide scientific discourse through defining government reference vehicles that contain functionally relevant artifacts but are not sensitive to specific developmental programs (see Army-Navy Basic Finner missile,[3-8] Air Force Modified Basic Finner missile,[3-8] Army-Navy Spinner Rocket,[8] National Aerospace Plane,[9] and NASA studies[10,11]). The goal of this report is to define a canonical, Army-relevant configuration suitable for foundational research to allow for focused collaboration with a critical mass of appropriate subject matter experts. Data and knowledge gained from studies on this open geometrical configuration may be subject to more restrictive distribution.

2. Vehicle Description

The High-Speed Army Reference Vehicle (HARV) is a symmetric flight vehicle that has an overall length-to-diameter of 10. The vehicle was initially shaped through a series of optimization analyses that identified design candidates with low drag and high lift-to-drag ratios. A more detailed description of the optimization process can be found in Vasile et al.[12,13] Several design iterations to simplify model fabrication and wind tunnel experimentation resulted in the establishment of HARV. The flight vehicle was designed for a modular forebody as well as aftbody-fin shapes to allow researchers to study a wide variety of phenomena.

The body section was a constant diameter cylinder. The diameter of the cylindrical body section is defined as 1 cal. Two nose profiles were studied, a cone and a Von Kármán ogive. The profile shapes for both cone and ogive were described using generic power series (i.e., n =1) and Haack series (i.e., C = 0), respectively, and computed as defined in Rosema.[14] The equivalent half angle of the conical nose is approximately 5°. The fineness ratio of both forebodies is 5. The nose tips for both forebodies were modeled with a spherical tip defined by a bluntness radius that is 0.05 of the base diameter (i.e., 0.05 cal.). An iterative scheme was necessary to solve the transition point from spherical tip to each prescribed nose profile to ensure a smooth transition (i.e., slope matching). Further details on the profile formulation are provided in the Appendix. The cross section for each nose profile shape is presented in Fig. 1. The forebodies allowed for studying the difference between boundary layers formed in favorable pressure gradients versus those without a pressure gradient.

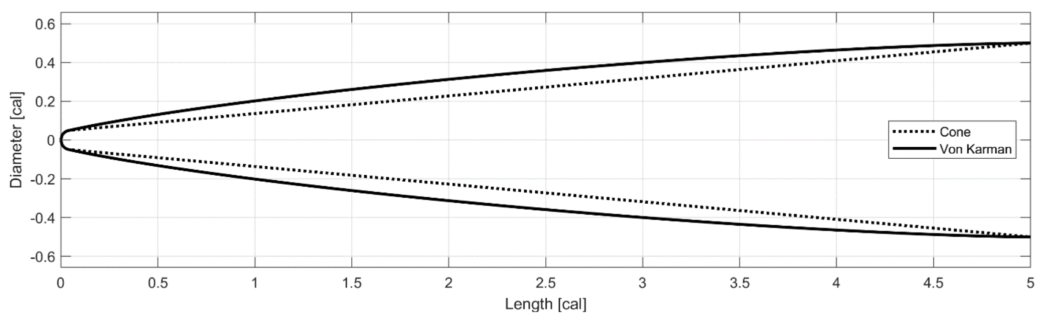

Fig. 1 HARV nose profile shapes

Two tail fin configurations were defined. The vehicle can be assembled using either three or four clipped-delta fins azimuthally separated 120° or 90°, respectively. The fin-body configurations allowed for investigating the effects of distance on fin-fin flow physics interactions. Each fin has a sweep angle of 80° and a root and tip chord length of 4.8 and 2.125 cal., respectively. Each fin has a uniform cross-sectional thickness of 0.07 cal. with a maximum tip semi-span of 0.95 cal. The leading edge was rounded using 0.03-cal. radii on either side of the fin with a flat section along the centerline with a width of 0.01 cal. Figure 2 shows additional details on the fin leading edge.

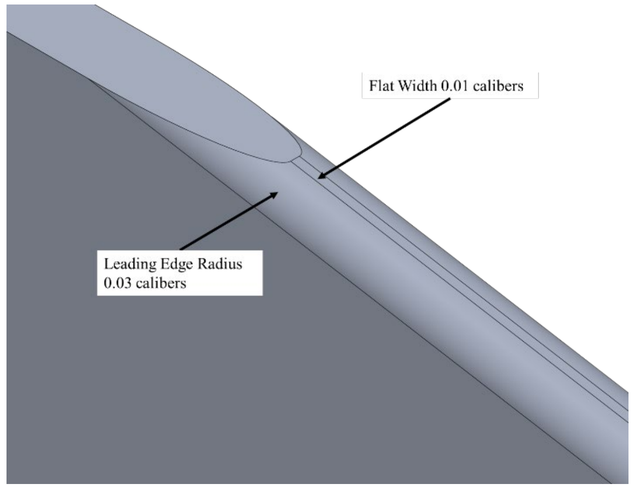

Fig. 2 HARV leading edge details common to all models. Zoomed view is where leading edge meets the fin tip.

The HARV for each unique configuration is illustrated in Figs. 3–6.

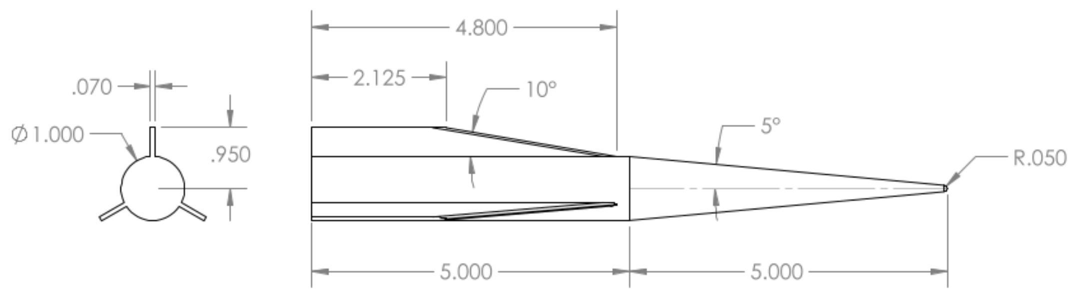

Fig. 3 HARV conical nose with three fins. All units are in calibers.

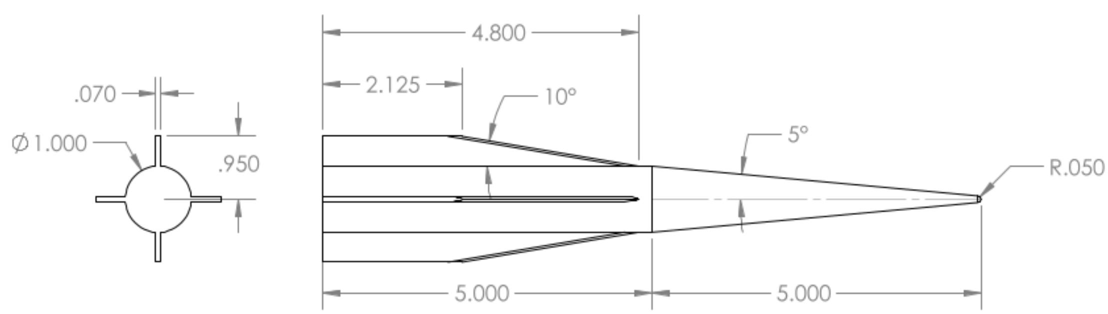

Fig. 4 HARV conical nose with four fins. All units are in calibers.

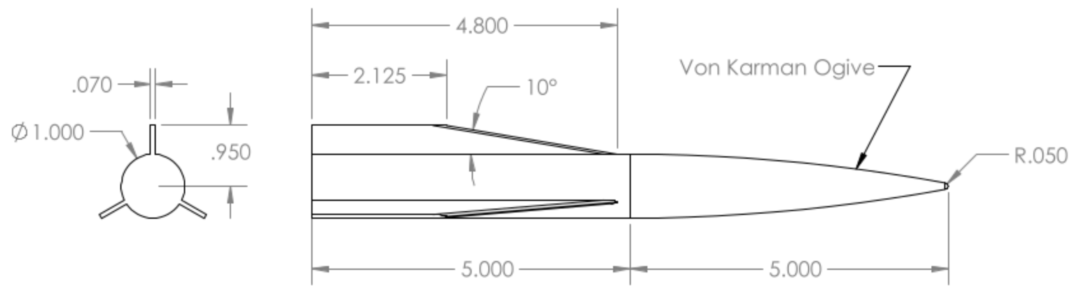

Fig. 5 HARV ogival nose with three fins. All units are in calibers.

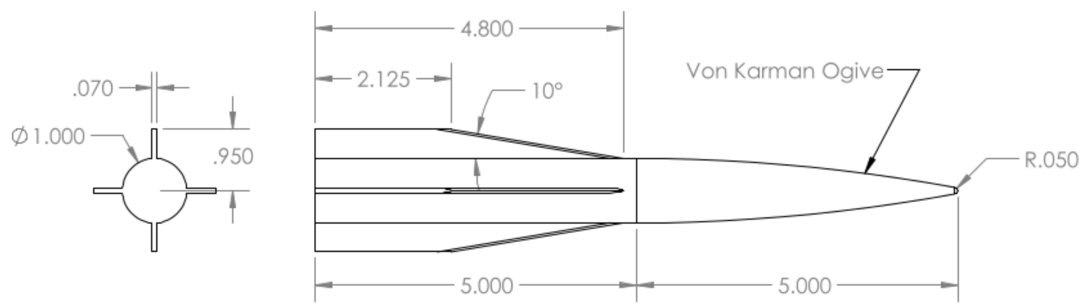

Fig. 6 HARV ogival nose with four fins. All units are in calibers.

The solid model rendering of the HARV for each unique configuration is presented in Figs. 7–10.

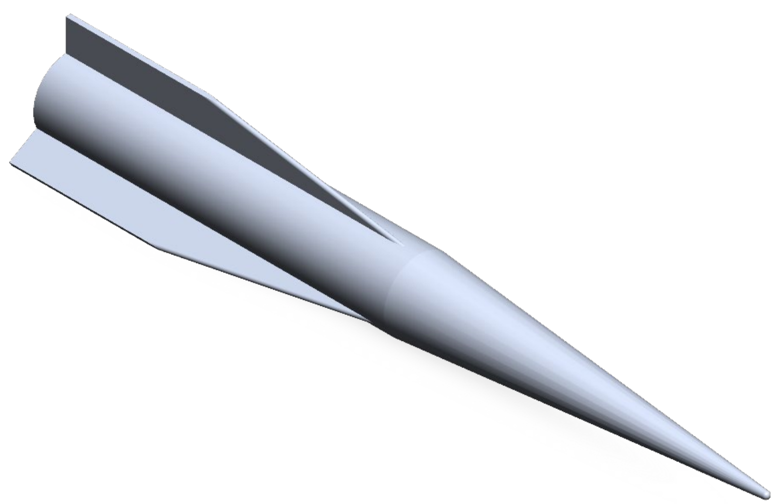

Fig. 7 HARV conical nose with three fins solid model rendering

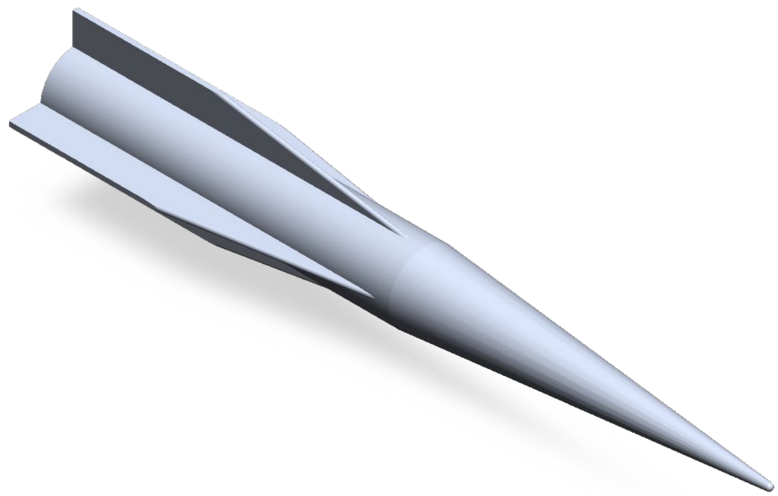

Fig. 8 HARV conical nose with four fins solid model rendering

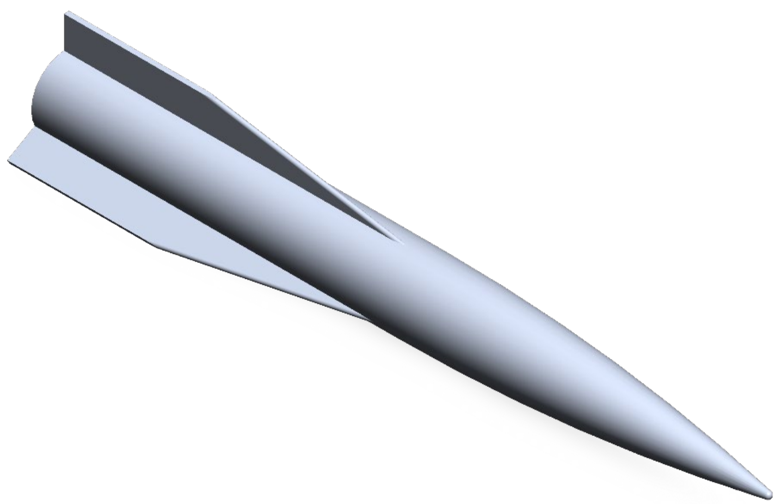

Fig. 9 HARV ogival nose with three fins solid model rendering

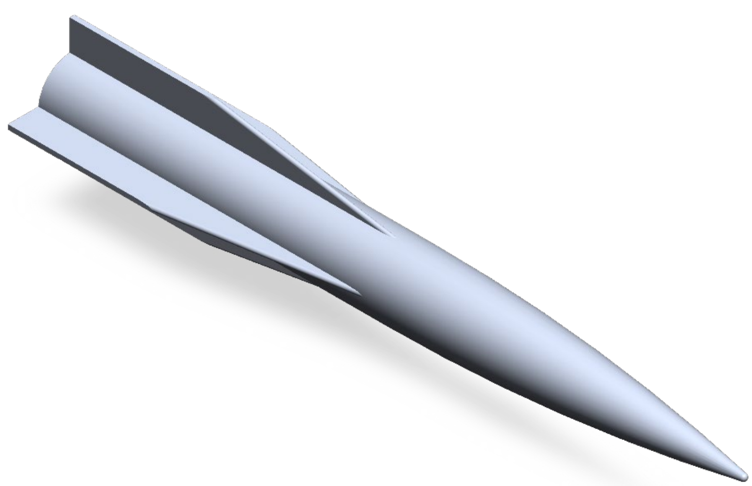

Fig. 10 HARV ogival nose with four fins solid model rendering

3. References

1. The U.S. Army in Multi-Domain Operations 2028; 2018 Dec 6. TRADOC Pamphlet 525-3-1.

2. Army Futures Command Concept for Fires 2028; 2021 Sep 15. AFC Pamphlet 71-20-6.

3. Jenke LM. Experimental roll-damping, magnus, and static-stability characteristics of two slender missile configurations at high angles of attack (0-90 deg) and mach numbers 0.2 through 2.5. Arnold Engineering and Development Center (US); 1976 July. Report No.: AEDC-TR-76-58.

4. Dupuis AD, Hathaway W. Aeroballistic range tests of the basic finner reference projectile at supersonic velocities. Defense Research Establishment; 1973 Aug. Report No.: DREV-TM-9703.

5. West KO. Comparison of free flight spark range and wind tunnel test data for a generic missile configuration at mach numbers from 0.6 to 2.5. Air Force Armament Laboratory (US); 1981 Oct. Report No.: AFATL-TR-81087.

6. Bhagwandin V. High-alpha prediction of roll damping and magnus stability coefficients for finned projectiles. Journal of Spacecraft and Rockets. 2016;53(4):720–729.

7. McCoy RL. Modern exterior ballistics. Schiffer Publications; 1999.

8. Murphy CH. Free flight motion of symmetric missiles. Army Ballistics Research Laboratory (US); 1963. Report No.: BRL-1216.

9. Williams RM. National aerospace plane – technology for America's future. Aerospace America. 1986;24(11):18–22.

10. Robinson RB, Bernot PT. Aerodynamic characteristics at a mach number of 6.8 of two hypersonic missile configurations, one with low-aspect-ratio cruciform fins and trailing-edge flaps and one with a flared afterbody and all-movable controls. National Advisory Committee for Aeronautics (US); 1958 Aug. Report No.: NACA RM L58D24.

11. Ashby GC, Fitzgerald PE. Longitudinal stability and control characteristics of missile configurations having several highly swept cruciform fins and a number of trailing-edge and fin-tip controls at mach numbers from 2.21 to 6.01. National Aeronautics and Space Administration (US); 1961 Jan. Report No.: TM X-355.

12. Vasile J, Bryson J, Fresconi F. Aerodynamic design optimization of long range projectiles using missile DATCOM. CCDC Army Research Laboratory (US); 2020. Report No.: ARL-TR-8936.

13. Vasile J, Bryson J, Fresconi F. Aerodynamic design optimization of long range projectiles using missile DATCOM. AIAA Scitech 2020 Forum; AIAA Paper 2020-1762, 2020.

14. Rosema C. Analysis of supersonic nose pressure drag using computational fluid dynamics. Army RDECOM AMRDEC (US); 2014. Report No.: RDMR-SS-13-14.

Appendix. Nose Profile Definition

A-1. Power Series Nose Profile

The blunted power series nose profile can be calculated through Fig. A-1 and subsequent content. (Figure and equations formulated from Rosema.[1])

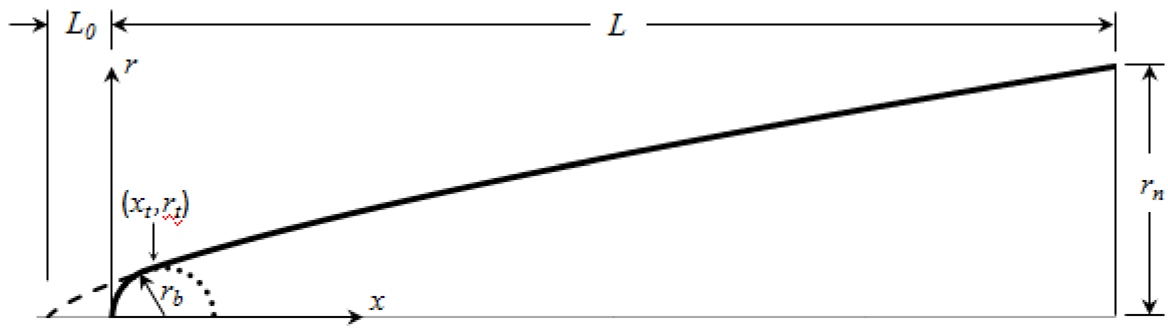

Fig. A-1 Definition of power series nose profile parameters

Basic power series relationship:

$$r(x) = r_n \left(\frac{x}{L}\right)^n$$

The equation for cone noses is formed by setting $n = 1$.

For the blunted tip,

$$r(x) = \sqrt{2xr_b - x^2}$$

For blunted cases, an iterative scheme is necessary to solve for the transition point, x_t.

Set an initial value for $r_t \approx 0.99r_b$ and let

$$t_1 = nr_t^2$$

$$t_2 = 1 - \left(\frac{r_t}{r_n}\right)^{1/n}$$

$$t_3 = \left(\frac{r_t}{r_n}\right)^{1/n}$$

$$t_4 = \sqrt{r_b^2 - r_t^2} + L - r_b$$

[1] Rosema C. Analysis of supersonic nose pressure drag using computational fluid dynamics. Army RDECOM AMRDEC (US); 2014. Report No.: RDMR-SS-13-14.

$$t_5 = \sqrt{r_b^2 - r_t^2}$$

and

$$\frac{dt_1}{dr_t} = 2nr_t$$

$$\frac{dt_2}{dr_t} = \frac{-1}{nr_n}\left(\frac{r_t}{r_n}\right)^{1/n-1}$$

$$\frac{dt_3}{dr_t} = -\frac{dt_2}{dr_t}$$

$$\frac{dt_4}{dr_t} = \frac{-r_t}{\sqrt{r_b^2 - r_t^2}}$$

$$\frac{dt_5}{dr_t} = \frac{dt_4}{dr_t}$$

then

$$f(r_t) = t_1 t_2 - t_3 t_4 t_5$$

and

$$f'(r_t) = t_1 \frac{dt_2}{dr_t} + t_2 \frac{dt_1}{dr_t} - t_3 t_4 \frac{dt_5}{dr_t} - t_3 t_5 \frac{dt_4}{dr_t} - t_4 t_5 \frac{dt_3}{dr_t}$$

The Newton-Raphson method may be used to solve for r_t:

$$r_t(i+1) \ = \ r_t(i) - \ n \frac{f\big(r_t(i)\big)}{f'\big(r_t(i)\big)}$$

where *n* is the relaxation factor and is usually set to a value of 0.1 for this case for stability.

Once r_t is known, x_t and L_0 can be solved for

$$x_t = r_b - \sqrt{r_b^2 - r_t^2}$$

$$L_0 = \frac{L\left(\frac{r_t}{r_n}\right)^{1/n} - x_t}{1 - \left(\frac{r_t}{r_n}\right)^{1/n}}$$

For $x \leq x_t$,

$$r(x) = \sqrt{2xr_b - x^2}$$

and for $x > x_t$,

$$r(x) = r_n\left(\frac{x + L_0}{L + L_0}\right)^n$$

A-2. Von Karman Nose Profile

The blunted Von Karman nose profile can be calculated through Fig. A-2 and subsequent content. (Figure and equations formulated from Rosema.[1])

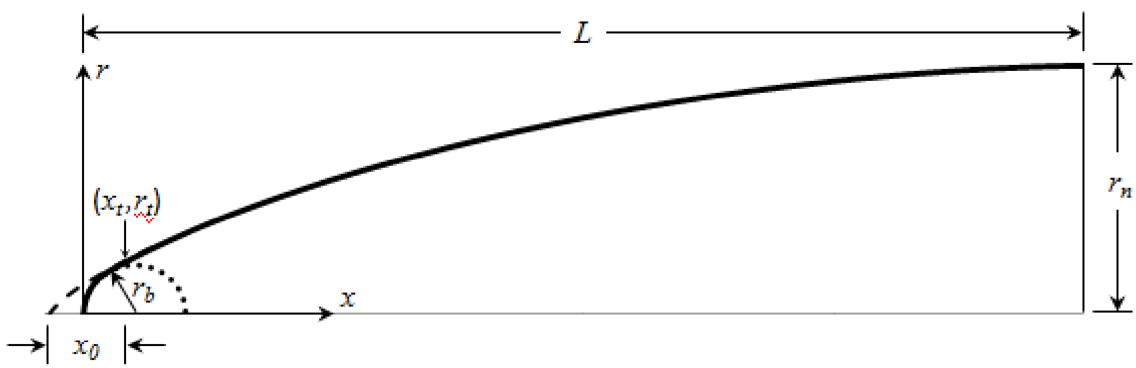

Fig. A-2 Definition of Von Karman nose profile parameters

The Von Karman profile is derived from the Sears–Haack series profile (i.e., C = 0):

$$r(x) = \frac{r_n\sqrt{\phi - \frac{\sin(2\phi)}{2}}}{\sqrt{\pi}}$$

where

$$\phi = \cos^{-1}\left(1 - \frac{2x}{L}\right)$$

For the blunted tip,

$$r(x) = \sqrt{2xr_b - x^2}$$

For blunted cases, a two-layer nested iterative scheme is necessary to solve for the transition point, x_t, and the offset length, x_0:

Set an initial value for $x_t \approx 0.97r_b$,

thus

$$r_t = \sqrt{2x_t r_b - x^2} = \frac{r_n \sqrt{\phi_t - \frac{\sin(2\phi_t)}{2}}}{\sqrt{\pi}}$$

Now iterate to solve for ϕ_t using the Newton–Raphson method where

$$f(\phi_t) = \frac{r_n \sqrt{\phi_t - \frac{\sin(2\phi_t)}{2}}}{\sqrt{\pi}} - r_t$$

and

$$f'(\phi_t) = \frac{r_n}{2\sqrt{\pi}} \frac{1 - \cos(2\phi_t)}{\sqrt{\phi_t - \frac{\sin(2\phi_t)}{2}}}$$

$$\phi_t(i+1) = \phi_t(i) - \frac{f\left(\phi_t(i)\right)}{f'\left(\phi_t(i)\right)}$$

The outer loop iterates on x_t to match the slopes at the transition point.

Let

$$L_h = L - x_t + x_0$$

where

$$x_0 = (L - x_t)\frac{1 - \cos(\phi_t)}{1 + \cos(\phi_t)}$$

Now let $f(x_t)$ equal the difference in the slopes of the two curves:

$$f(x_t) = \left.\frac{dr}{d\phi}\right|_{\phi=\phi_t} \left.\frac{d\phi}{dx}\right|_{x=x_0} - \frac{r_b - x_t}{r_t}$$

$$f'(x_t) = \left.\frac{dr}{d\phi}\right|_{\phi=\phi_t} \left.\frac{d^2\phi}{dx^2}\right|_{x=x_0} + \left(\left.\frac{d\phi}{dx}\right|_{x=x_0}\right)^2 \left.\frac{d^2r}{d\phi^2}\right|_{\phi=\phi_t} + \frac{1}{r_t} + \frac{(r_b - x_t)^2}{r_t^3}$$

where

$$\left.\frac{dr}{d\phi}\right|_{\phi=\phi_t} = \frac{r_n}{2\sqrt{\pi}} \frac{1-\cos(2\phi_t)}{\sqrt{\phi_t - \frac{\sin(2\phi_t)}{2}}}$$

$$\left.\frac{d\phi}{dx}\right|_{x=x_0} = \frac{1}{\sqrt{x_0 L_h - x_0^2}}$$

$$\left.\frac{d^2r}{d\phi^2}\right|_{\phi=\phi_t} = \frac{r_n}{2\sqrt{\pi}}\left(\frac{2\sin(2\phi_t)}{\sqrt{\phi_t - \frac{\sin(2\phi_t)}{2}}} - \frac{(1-\cos(2\phi_t))^2}{2\left(\phi_t - \frac{\sin(2\phi_t)}{2}\right)^{3/2}}\right)$$

$$\left.\frac{d^2\phi}{dx^2}\right|_{x=x_0} = \frac{2x_0 - L_h}{2(x_0 L_h - x_0^2)^{3/2}}$$

And finally

$$x_t(i+1) = x_t(i) - n\frac{f\left(x_t(i)\right)}{f'\left(x_t(i)\right)}$$

where $0 < n \le 1$, but $n = 0.01$ is recommended

For $x \le x_t$,

$$r(x) = \sqrt{2xr_b - x^2}$$

and for $x > x_t$,

$$r(x) = \frac{r_n\sqrt{\phi - \frac{\sin(2\phi)}{2}}}{\sqrt{\pi}}$$

where

$$\phi = \cos^{-1}\left(1 - \frac{2(x - x_t + x_0)}{L_h}\right)$$

1 (PDF) DEFENSE TECHNICAL INFORMATION CTR
DTIC OCA

1 (PDF) DEVCOM ARL
FCDD RLD DCI
TECH LIB

1 (PDF) JHU/APL
B WHEATON

1 (PDF) SANDIA NATIONAL LABS
C SMITH

3 (PDF) TAMU
R BOWERSOX
E WHITE
H REED

2 (PDF) PURDUE
C SCALO
J POGGIE

2 (PDF) DEVCOM AC
M DUCA
T RECCHIA

1 (PDF) DAC
G MANNIX

6 (PDF) DEVCOM AVMC
B GRANTHAM
J DOYLE
C ROSEMA
M MCDANIEL
P CROSS
L AUMAN

40 (PDF) DEVCOM ARL
FCDD RLW A
F FRESCONI
FCDD RLW WD
J VASILE
J DESPIRITO
FCDD RLW
J ZABINSKI
FCDD RLW A
F FRESCONI
FCDD RLW L
W OBERLE
P PEREGINO
T SHEPPARD
FCDD RLW LB
N TRIVEDI
E BYRD
FCDD RLW LC
J SADLER
FCDD RLW LD
A WILLIAMS
M NUSCA
A MCBAIN
FCDD RLW LE
J VASILE
J BRYSON
J DESPIRITO
L STROHM
J PAUL
V BHAGWANDIN
L FAIRFAX
B GRUENWALD
I CELMINS
J SAHU
FCDD RLW LF
M ILG
B TOPPER
D EVERSON
T BROWN
FCDD RLW LH
M MINNICINO
FCDD RLW V
S SILTON
V BLAIR
J CAIN
D KNORR
K BEHLER
J TZENG
L BRAVO
A GHOSHAL
M MUTHUVEL
J OGRADY
N REICHENBACH